First-Principles Calculation of Laser Crystal Multiplet Levels via Hybridized Density Functional Theory and Configuration Interaction within the OLCAO Method

Benjamin Walker

University of Missouri – Kansas City, 257 Flarsheim Hall, 5110 Rockhill Road, Kansas City, Missouri, 64110

baw5ea@mail.umkc.edu

Abstract. Computation of highly-localized multiplet energy levels of transition metal dopants is essential to the design of materials such as laser host crystals. A purely first-principles density functional theory-configuration interaction (DFT-CI) hybrid computational method has been developed to accurately compute multiplet energy levels for single atoms of carbon, nitrogen, oxygen, sodium, aluminum, silicon, titanium, and chromium. The multiplet energy levels have been computed with close experimental agreement in terms of magnitude and degeneracy, and the method does not depend on empirical information (i.e. Racah parameters). The computed multiplet energy level results are distributed according to term symbols, which are then compared to experimentally-observed multiplet energy levels. The hybrid method consists of analytic computation of two-electron integrals via the DFT-based orthogonalized linear combination of atomic orbitals (OLCAO) method, which are subsequently used as input for the CI-based discrete variational multi-electron (DVME) method to obtain the multiplet energy values.

Keywords: exchange-correlation; elecron repulsion integral; multiplet; DVME; OLCAO; density functional theory; configuration interaction

1. Introduction

A key driving economic force over the past few decades has been the development of advanced materials with novel and/or highly tuned properties. This trend is expected to continue into the future due to tough global competition for manufactured products, new technologies, and the demand for progress in fundamental science. Many manufactured products and new technologies rely heavily on subtle details of the electronic structures of the component materials. In order to achieve optimal performance within the constraints (e.g. thermal, mechanical, form factor, *etc*.) imposed by the specific application it is necessary to possess fundamental understanding of the material. A few general application examples include photovoltaics, laser host crystals, photo-detectors, lighting phosphors, and quantum dots [1–5]. Specific areas of fundamental physical importance are excitonic states, electron mobility, electron-phonon coupling, and precise band structure including multiplet and satellite energy levels [6–8]. These applications and points of fundamental research are intimately associated with excitations of the valence band electrons into the unoccupied conduction band states. Therefore, an area of particularly urgent research interest is the ability to make an accurate determination of the excited state properties of materials with an emphasis on those containing doped atoms with *3d*, *4d*, and *4f* valence electrons

because they tend to possess the most uniquely tunable properties. The presence of such dopant atoms within a solid introduces additional highly localized electronic states into the gap between the occupied and unoccupied states. Figure 1 shows a comparison between the band structures of undoped Al_2O_3 and chromium-doped Al_2O_3 (ruby).

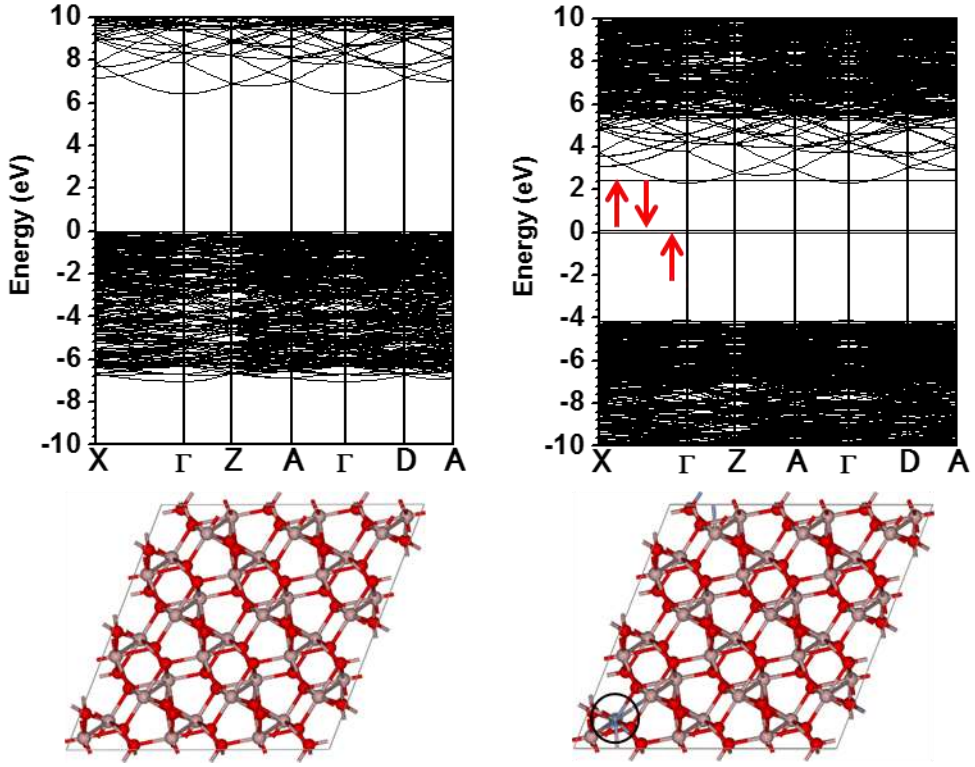

Figure 1. α-Al_2O_3 band structure example. α-Al_2O_3 with and without dopant. Left: Supercell band and crystal structure of α-Al_2O_3. Right: As the left side with a Cr substitutional defect (circled). Induced multiplet states are identified by arrows.

Experimental spectroscopic techniques to study these types of materials systems have progressed very far in recent decades, but it is clear that fundamental understanding and efficient analysis is only achieved when theoretical and computational methods are applied as well. In response to this need, tremendous effort has been expended to develop and apply such methods [9,10]. At present, computational theoretical methods have proven themselves to be extremely cost effective, efficient, and powerful tools. However, as with experiment, each computational method has its own set of advantages and disadvantages in terms of capability, accuracy, and efficiency. In fact, increased accuracy tends to come at the cost of efficiency, and vice versa. A prime example is that many methods need to explicitly compute the excited state electronic wave function for accurate prediction of the spectral properties of a material. Such an explicit wave function calculation has never been feasible for bulk solids due to the high computational cost involved; rather it has been used with smaller molecule-sized systems. While progress has been made, very substantial challenges remain in addressing these disadvantages and will likely require many more years of focused effort.

An example is the case of ruby; it has three lines (R, R', B) and three bands (U, Y, Y') in the visible spectrum which correspond to multiplets of impurity states. There have been studies that successfully computed multiplet levels from first principles. For example, Ohnishi and Sugano [11] computed two multiplet states of ruby, ^2E (R line) and $^4T_2$ (U band). In 1998 Prof. Ogasawara et al.[12] calculated the multiplet structure of ruby via a many-electron extension of the DV-Xα method [13] (Figure 2) thereby

elucidating the effects that covalency and trigonal distortion of the impurity-state wave function have on the multiplet structure of ruby.

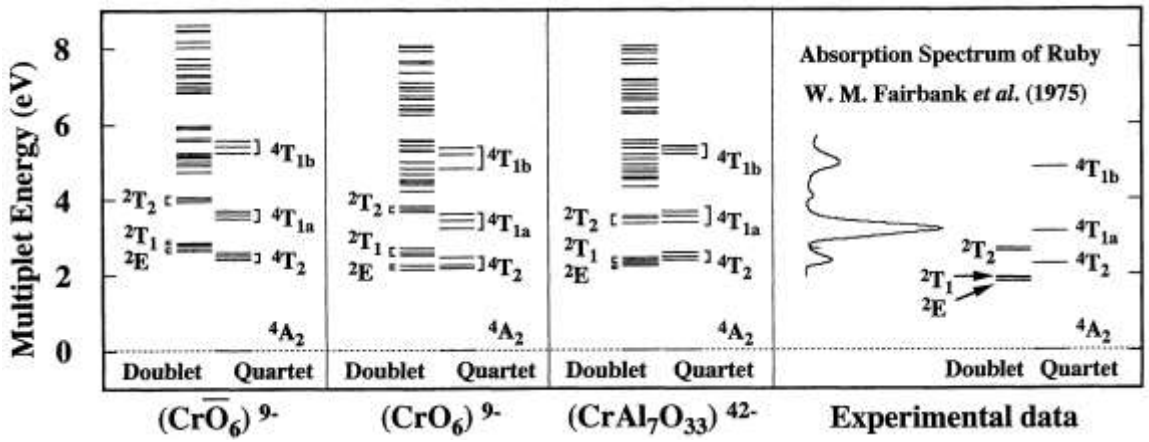

Figure 2. Ruby multiplet energy levels. Calculated multiplet energy levels of ruby using three different clusters, in comparison with the experimental absorption spectrum [14].

As is shown in Figure 2, there is a significant difference between the computed multiplet states of ruby, and those observed experimentally. For example, computed ^2E, $^2T_1$ and $^4T_2$ multiplet energy levels differ from their experimental counterparts in terms of quantity and magnitude. This difference is due to the presence of correlated electron-electron interactions that are not properly accounted for in the calculation.

The current state of the art in predicting laser crystal multiplet energy levels is to plot them with Tanabe-Sugano diagrams [15,16]. In this method, an approximation of the crystal field splitting energies as a function of ligand field strength is generated for tetrahedral or octahedral complexes. For instance, the *d*-orbital energy levels of neutral transition metals are degenerate, but in the presence of ligands the degeneracy of the energy levels is broken when crystal splitting occurs (denoted by Δ_{oct}).

Ruby is represented by an octahedral complex wherein a chromium atom is surrounded by six oxygen atoms. The energies of the $d_{xx\text{-}yy}$ and d_{zz} orbitals increase relative to those of the d_{xy}, d_{xz}, and d_{yz} orbitals. The energy splittings are characterized by empirically-determined Racah parameters [17] (denoted by *B* and *C*), which are meant to account for electron-electron repulsion. In this case, *B* represents the bond strength between the metal ion and the ligand, and is used to defined *C* as 1/4*B*. A Tanabe-Sugano diagram consists of the energy of an electron transition scaled by *B*, as a function of the crystal field splitting parameter Δ_{oct}, also scaled by *B*. While accurate, Tanabe-Sugano diagrams are dependent on empirically-derived Racah parameters. This work provides a framework for a method that is not dependent on the inclusion of empirical parameters to calculate multiplet energy levels. However, key challenges need to be addressed.

The essence of the problem being addressed in this work is that the excited state electronic properties of a solid can only be precisely described when correlated electron-electron interactions are taken into account. In strongly-correlated systems, atoms with partially occupied *d* and/or *f* electron shells exhibit atom-like behavior, thereby limiting the accuracy of the homogeneous electron gas model employed by LDA- and GGA-based methods. The situation becomes even more complicated when electrons are excited into higher energy levels, because the excitation changes the electronic structure of the entire system. Electron-electron interaction phenomena cannot be decoupled from each other, which precludes direct calculation of their effects. However, the effects can collectively be accounted for via the strategic application of suitable computational methods – in effect, a hybrid method.

2. Methods

2.1. DVME

The discrete variational multi-electron (DVME) method that is used for this work was developed in 2000 and has been successfully used to compute multiplet states for ruby [18-20]. In that work, an effective Hamiltonian was employed that takes only dopant-state electrons explicitly into account:

$$H = \sum_{i=1}^{M} h\left(\vec{r}_i\right) + \sum_{i} \sum_{j<i} g\left(\vec{r}_i, \vec{r}_j\right) \tag{1}$$

Here, $\vec{r}_i$ is the position of the i^{th} electron and M is the number of electrons occupying dopant states. The first term in the effective Hamiltonian is the one-electron operator:

$$h\left(\vec{r}\right) = -\frac{1}{2}\nabla^2 + V_{ext}\left(\vec{r}\right) + V_0\left(\vec{r}\right) \tag{2}$$

This is composed of the following terms: ∇^2 is the kinetic energy term, $V_{ext}\left(\vec{r}\right)$ is the Coulombic potential from surrounding nuclei, and $V_0\left(\vec{r}\right)$ is the Coulombic repulsion energy from the core and valence electrons. The second term in the effective Hamiltonian is the two-electron operator:

$$g\left(\vec{r}_i, \vec{r}_j\right) = \frac{1}{\left|\vec{r}_{ij}\right|} \tag{3}$$

where $\vec{r}_{ij}$ is the distance between the i^{th} and j^{th} impurity state electrons.

According to the prior work of Prof. Ogasawara, Slater determinants Φ_i, representing the impurity state orbitals, are constructed via the single-electron cluster calculation described in 2000[18]. Determination of the energy levels of the impurity states starts with diagonalizing the effective Hamiltonian within the subspace spanned by Φ_i. Next, the matrix elements of the Hamiltonian H are expanded to obtain:

$$H_{pq} = \left\langle \Phi_p \left| H \right| \Phi_q \right\rangle = \sum_{i=1}^{L}\sum_{j=1}^{L} A_{ij}^{pq} \left\langle i \left| h \right| j \right\rangle + \sum_{i=1}^{L}\sum_{j=1}^{L}\sum_{k=1}^{L}\sum_{\ell=1}^{L} B_{ijkl}^{pq} \left\langle ij \left| g \right| kl \right\rangle \tag{4}$$

where L is the number of impurity state orbitals, A and B are coefficients, and Φ_i are Slater determinants constructed from impurity state orbitals obtained from the CI cluster calculation. Additionally, $\left\langle i \mid h \mid j \right\rangle$ is the one-electron integral, and $\left\langle ij \mid g \mid kl \right\rangle$ is the two-electron integral, also known as the electron repulsion integral (ERI). These integrals are defined as follows:

$$\left\langle i \left| h \right| j \right\rangle = \int \phi_i^*\left(\vec{r}\right) h\left(\vec{r}\right) \phi_j\left(\vec{r}\right) d\vec{r} \tag{5}$$

$$\left\langle ij \left| g \right| kl \right\rangle = \int\int \phi_i^*\left(\vec{r}_1\right) \phi_j^*\left(\vec{r}_2\right) \frac{1}{\left|r_{12}\right|} \phi_k\left(\vec{r}_1\right) \phi_l\left(\vec{r}_2\right) d\vec{r}_1 d\vec{r}_2 \tag{6}$$

In these integrals, the ϕ terms represent impurity-state orbitals. Next, eigenvectors are obtained to express the many-electron impurity state wave function:

$$a_{n1}, a_{n2}, \cdots, a_{nK} \tag{7}$$

$$\Psi_n = a_{n1}\Phi_1 + a_{n2}\Phi_2 + \cdots + a_{nK}\Phi_K \tag{8}$$

where *K* is the number of Slater determinants. This is the CI formalism defined in the previous section. *H* is diagonalized in terms of Ψ_n to obtain the energy of the n^{th} eigenstate:

$$E^n = \left\langle \Psi_n \middle| H \middle| \Psi_n \right\rangle = \sum_p^K \sum_q^K a_{np}^* a_{nq} H_{pq} \tag{9}$$

A major distinction to be made between the DVME method as shown here and the work being presented in this dissertation is how the ERIs are computed. The stand-alone DVME method computes ERIs numerically[18] via random sampling points, a method that is less accurate than analytical computation; furthermore, it is and exceedingly expensive calculation for large systems. The hybrid DFT-CI method of this dissertation removes this complication by analytically computing the ERI solutions and substituting them into the effective Hamiltonian to be used in the aforementioned DVME procedure. The ERI derivation is shown in the subsequent section on interaction integrals.

The Hartree-Fock method and its derivatives rely on direct computation of the wave function of the system being studied. In the next section an alternative approach in the form of density function theory will be discussed, with subsequent discussion about how the hybrid DFT-CI method is formed.

2.2. Orthogonalized Linear Combination of Atomic Orbitals (OLCAO) Method

Over the past several decades, meeting the challenge of calculating the properties of materials has been made possible by the emergence of powerful and efficient computer and algorithms. The DFT-based OLCAO method [21] has been shown to be accurate and efficient for large periodic atomic systems [19,21]. The OLCAO method employs a basis of atom-centered atomic orbitals that are expanded as Gaussian functions, which facilitates accurate and efficient computation of interaction integrals.

Atomic Basis Functions

The solid state wave function $\Psi_{n\vec{k}}(\vec{r})$ for energy band index *n* and wave vector $\vec{k}$ is defined as:

$$\Psi_{n\vec{k}}(\vec{r}) = \sum_{i,\gamma} C_{i\gamma}^n(\vec{k}) b_{i\gamma}(\vec{k},\vec{r}) \tag{10}$$

For the i^{th} aggregated quantum number (principle, angular momentum, and magnetic) and the γ^{th} atom in the cell. The Bloch sum $b_{i\gamma}(\vec{k},\vec{r})$ is defined as:

$$b_{i\gamma}(\vec{k},\vec{r}) = \frac{1}{\sqrt{N}} \sum_{\upsilon} \exp\left[i\left(\vec{k}\cdot\vec{R}_\upsilon\right)\right] u_i\left(\vec{r}-\vec{R}_\upsilon-\vec{t}_\gamma\right) \tag{11}$$

where $\vec{R}_v$ is the lattice vector and $\vec{t}_\gamma$ is the position of the γ^{th} atom. The sum over υ of u_i represents an atom-centered linear combination of atomic orbitals. Each atomic orbital consists of a radial part and an angular part:

$$u_i(\vec{r}) = \left[\sum_{j=1}^N A_j r^l \exp\left(-\alpha_j r^2\right)\right] \cdot Y_l^m(\theta,\phi) \tag{12}$$

where *l* and *m* are angular momentum quantum numbers and A_j are expansion coefficients. The *N* decay factors α_j of the sum of Gaussian-type orbitals (GTOs) are selected by empirically choosing minimum and maximum values and then obtaining the rest via a geometric series between them. During an OLCAO calculation, the same set $\{\alpha_j\}$ is used for all the atoms of a given element, as well as for all the orbitals for a given quantum number *i*. In this way, the basis functions are element-specific and predetermined. Because of this, interaction integrals are computed and reused.

The OLCAO method is based on the local density approximation (LDA) of density functional theory (DFT). Next, the Kohn-Sham equation for a system of interacting particles is obtained:

$$\left[-\vec{\nabla}^2 + V_{e-n}\left(\vec{r}\right) + V_{e-e}\left(\vec{r}\right) + V_{XC}\left[\rho\left(\vec{r}\right)\right]\right]\Psi_{n\vec{k}}\left(\vec{r}\right) = E_{n\vec{k}}\Psi_{n\vec{k}}\left(\vec{r}\right) \tag{13}$$

where $V_{e-n}\left(\vec{r}\right)$ represents the electron-nuclear potential, $V_{e-e}\left(\vec{r}\right)$ represents the electron Coulombic potential, and $V_{XC}\left[\rho\left(\vec{r}\right)\right]$ represents the exchange-correlation (XC) potential energy. The XC potential has a functional relationship to the charge density $\rho\left(\vec{r}\right)$. Here, $\rho\left(\vec{r}\right)$ is the electron density over occupied states:

$$\rho\left(\vec{r}\right) = \sum_{occ}\left|\Psi_{n\vec{k}}\left(\vec{r}\right)\right|^2 \tag{14}$$

The total energy of the system is:

$$E_T = \sum_{n,\vec{k}}^{occ} E_n\left(\vec{k}\right) + \int \rho\left(\vec{r}\right)\left(\varepsilon_{XC} - V_{nuc-e} - \frac{V_{e-e}}{2}\right)d\vec{r} + \frac{1}{2}\sum_{\gamma,\delta}\frac{Z_\gamma Z_\delta}{\vec{R}_\gamma - \vec{R}_\delta} \tag{15}$$

The first term is the sum of energies over occupied one-electron bands; within the middle term: ε_{XC} is XC energy, V_{nuc-e} is nucleus-electron attraction energy, and $\frac{V_{e-e}}{2}$ is electron-electron repulsion energy; the last term is a sum of nucleus-nucleus repulsion energy over the lattice sites, where δ and γ are lattice sites and Z_δ and Z_γ are atomic numbers at lattice sites δ and γ.

Atom-Centered Potentional Functions

The real-space charge distribution $\rho_{cry}\left(\vec{r}\right)$ for an OLCAO calculation is defined as follows:

$$\rho_{cry}\left(\vec{r}\right) = \sum_A \rho_A\left(\vec{r} - \vec{t}_A\right) \tag{16}$$

where:

$$\rho_A\left(\vec{r}\right) = \sum_{j=1}^{N} B_j \exp\left(-\beta_j \vec{r}^2\right) \tag{17}$$

The atom-centered Coulomb potential $V_{Coul}\left(\vec{r}\right)$ is expressed as follows:

$$V_{Coul}\left(\vec{r}\right) = \sum_A V_C\left(\vec{r} - \vec{t}_A\right) \tag{18}$$

where $V_C\left(\vec{r}\right)$ is defined as

$$V_C\left(\vec{r}\right) = -\frac{Z_A}{\left|\vec{r}\right|}\exp\left(-\varsigma r^2\right) - \sum_{j=1}^{N} D_j \exp\left(-\beta_j \vec{r}^2\right) \tag{19}$$

The first term represents the electron-nuclear potential, where Z_A is the atomic number of the atom at the nucleus site; the second term of $V_C\left(\vec{r}\right)$ is the electron-electron potential.

The exchange-correlation potential $V_{XC}\left(\vec{r}\right)$ is defined as

$$V_{xc}\left(\vec{r}\right) = \sum_A V_x\left(\vec{r} - \vec{t}_A\right) \tag{20}$$

where:

$$V_x(\vec{r}) = \sum_{j=1}^{N} F_j \exp\left(-\beta_j \vec{r}^{\,2}\right) \tag{21}$$

The crystal potential is defined as a sum of the above atom-centered potentials:

$$V_{cry}(\vec{r}) = \sum_A V_A(\vec{r} - \vec{t}_A) \tag{22}$$

where:

$$V_A(\vec{r}) = V_C(\vec{r}) + V_x(\vec{r}) \tag{23}$$

The same set of exponential decay parameters $\{\beta_j\}$ is used in the above Gaussian functions. This allows for reuse of the expanded Gaussian functions $\exp\left(-\beta_j \vec{r}^{\,2}\right)$, hence fewer integral computations need to be performed. The mathematical form of $\rho_A(\vec{r})$ and $V_A(\vec{r})$ allows for the analytical computation of multicenter interaction integrals, which is a factor that lends to the computational efficiency of OLCAO.

Gaussian-Type Orbitals (GTOs)

Computation of symmetric band structure about the Brillouin zone is accomplished by solving the secular equation:

$$\left| H_{i\gamma,j\delta}(\vec{k}) - S_{i\gamma,j\delta}(\vec{k}) E(\vec{k}) \right| = 0 \tag{24}$$

where:

$$\begin{aligned} S_{i\gamma,j\delta}(\vec{k}) &= \left\langle b_{i\gamma}(\vec{k},\vec{r}) \,|\, b_{j\delta}(\vec{k},\vec{r}) \right\rangle \\ &= \sum_\mu \exp\left(-i\vec{k}\cdot\vec{R}_\mu\right) \int u_i(\vec{r} - \vec{t}_\gamma)\, u_j(\vec{r} - \vec{R}_\mu - \vec{t}_\delta)\, d\vec{r} \end{aligned} \tag{25}$$

and:

$$\begin{aligned} H_{i\gamma,j\delta}(\vec{k}) &= \left\langle b_{i\gamma}(\vec{k},\vec{r}) \,|\, H \,|\, b_{j\delta}(\vec{k},\vec{r}) \right\rangle \\ &= \sum_\mu \exp\left(-i\vec{k}\cdot\vec{R}_\mu\right) \int u_i(\vec{r} - \vec{t}_\gamma) \left[-\nabla^2 + V_{Coul}(\vec{r}) + V_{ex}(\vec{r}) \right] u_j(\vec{r} - \vec{R}_\mu - \vec{t}_\delta)\, d\vec{r} \end{aligned} \tag{26}$$

where $\vec{k}$ represents a set of ***k***-points. Even for larger systems of hundreds or thousands of atoms, the number of interaction integrals that need to be computed remains manageable due to the reuse of interaction integrals.

With the atom-centered potentials in-hand, let u_i be an s-type ($\ell = 0$) Gaussian function with decay parameter α_1, centered at atomic site *A*:

$$|\phi_A\rangle = \exp\left(-\alpha_1 \vec{r}_A^{\,2}\right) \tag{27}$$

where $\vec{r}_A = \vec{r} - \vec{A}$. OLCAO has a basis of Gaussian-type orbitals (GTOs), which is advantageous compared to other basis sets (i.e. plane wave basis). For example, a plane wave basis set requires many terms in order to accurately expand a wave function, making such bases more mathematically intense to compute. Gaussian functions are analytically integrated and differentiated easily.

Creating the OLCAO-DVME Hybrid Method

The first step in the hybrid calculation process is to accumulate the analytically computed single electron integrals and electron repulsion integrals with the OLCAO method. Single electron integrals consist of a sum of kinetic energy and nuclear attraction integral matrix elements. For the sake of brevity in describing the hybrid OLCAO-DVME method, single electron integrals and electron repulsion integrals are referred to as 'single integrals' and 'double integrals', respectively. To demonstrate how the single and double integrals are accumulated in OLCAO, the accumulation process for 2-center overlap integrals is shown here first.

Each atomic site has an atom-centered Gaussian function $|\phi_A\rangle = \exp\left(-\alpha_1 \vec{r}_A^{\,2}\right)$ with decay parameter α. Each alpha has a set of atomic orbitals (1s, 2s, $2p_x$, $2p_y$, $2p_z$, *etc*.), and the total number of valence orbitals for all the atoms in a given system is known as the valence dimension. When performing stand-alone OLCAO calculations, it is often preferable to consider only non-core electronic states. However, when preparing an OLCAO-DVME calculation, both core and valence orbitals are included in the single and double integrals.

In the case of 2-center overlap integrals, all pairs of alphas (without double counting) are tested for non-negligible Gaussian overlap (highlighted portion of the schematic of Figure 3.

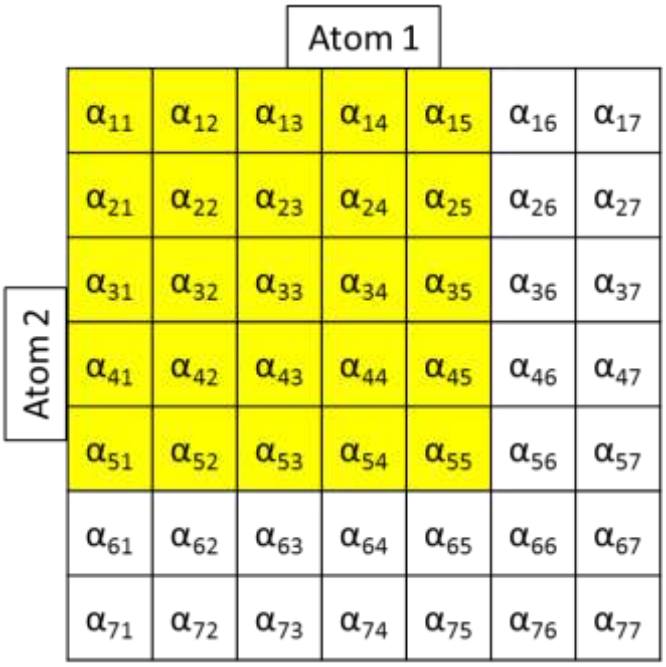

Figure 3. Alpha pairs: highlighted are alphas involved in non-negligible overlap.

When this condition is met, the overlap integral subroutine is called for the alpha pair taking part in the non-negligible overlap. For each pair, the angular momentum character of the Gaussian function for the second alpha (α_2) determines the number of states over which the overlap is accumulated. This number is either 1, 4, 9, or 16 corresponding to *s*-, *p*-, *d*-, or *f*-type orbitals; this number is the upper bound on the accumulation loop. Starting from zero, each iteration of the loop adds the product of the orbital overlap of α_1 multiplied by each of the set of α_2. Once all the alphas are looped over, the integral with a complete basis representation is formed. This formalism is applied to 2-center overlap,

kinetic energy, 3-center electronic potential, and 3-center nuclear attraction integrals. Next, the single integrals are computed.

Single integrals are a term-by-term sum of the complete basis representation of kinetic energy and nuclear attraction integral matrix elements. The algorithm is as follows:

$$\begin{aligned}
&\mathrm{One}(\mathrm{i},\mathrm{j}) = 0\\
&\text{do i=1,valeDim}\\
&\text{do j=1,valeDim}\\
&\mathrm{One}(\mathrm{i},\mathrm{j}) = \left[\mathrm{KE}(\mathrm{i},\mathrm{j}) + \mathrm{NP}(\mathrm{i},\mathrm{j})\right]\\
&\text{write One}(\mathrm{i},\mathrm{j})\\
&\text{end do}\\
&\text{end do}
\end{aligned}$$

The algorithm for double integrals is as follows:

$$\begin{aligned}
&\mathrm{Two}(\mathrm{i},\mathrm{j},\mathrm{k},\ell) = 0\\
&\text{do i=1,valeDim}\\
&\text{do j=1,valeDim}\\
&\text{do k=1,valeDim}\\
&\text{do } \ell\text{=1,valeDim}\\
&\mathrm{Two}(\mathrm{i},\mathrm{j},\mathrm{k},\ell) = \mathrm{ERI}(\mathrm{i},\mathrm{j},\mathrm{k},\ell)\\
&\text{write Two}(\mathrm{i},\mathrm{j},\mathrm{k},\ell)\\
&\text{end do}\\
&\text{end do}\\
&\text{end do}\\
&\text{end do}
\end{aligned}$$

The accumulated single and double integrals are used as input for DVME to perform a CI-style calculation that computes energy eigenvalues. It is important to note that the nuclear attraction integral within DVME treats the nucleus site as a point charge, whereas the nucleus site is treated with an *s*-type Gaussian function in OLCAO. Therefore, OLCAO-generated nuclear attraction integrals for use in the hybrid method are prepared in the DVME style. This means that the application of the Gaussian Product Theorem and factoring of constants is the same as for the 2-center overlap integral.

3. Results and discussion

The main result of this work is the development of a purely first-principles method for computing the multiplet energy levels of single atoms, specifically transition metal dopants within crystalline systems. Such a method has remained elusive due to the reduced accuracy of DFT-based methods when applied to strongly correlated systems, as well as the prohibitive computational expense in applying post-HF methods to periodic crystals. However, strategic application of both methods at different stages of a hybrid-style calculation has shown promising results.

The method computes atomic energy levels within the ground-state electron configuration. The multiplet energy values for atoms are distributed according to term symbols that have the form ${}^{2S+1}L_J$,

where S is the total spin quantum number, L is the total orbital quantum number, and J is the total angular momentum quantum number [22]. For a given pair of electrons within a subshell, we know that $L=|\ell_1-\ell_2|$ to $\ell_1+\ell_2$, $S=|s_1-s_2|$ to s_1+s_2, and $J=|L-S|$ to $L+S$. The value of L determines the letter code of the term symbol, such that $L=0$ corresponds to S, $L=1$ corresponds to P, *etc*. in the same way as orbitals are designated. Spin degeneracy is determined from the fact that each level has $2S+1$ states. One additional constraint is that the many-electron wave function must be anti-symmetric when considering the combination of spin and orbital angular momenta.

Putting this formalism into practice for Sodium, the single unpaired electron in the 3s subshell allows for straightforward tabulation of the ground-state term symbols. We have $S=\frac{1}{2}$, $L=0$, and $J=\frac{1}{2}$; this means we expect that there is a single anti-symmetric term $^2S_{1/2}$ for ground-state Sodium, with this state being doubly spin degenerate (containing $2S+1=2\left(\frac{1}{2}\right)+1=2$ states). This is in agreement with what has been observed experimentally [23], and is summarized in Table 1:

Table 1. Sodium multiplet energies (eV)

Term Symbol	OLCAO-DVME Method	DVME	Term Symbol	Experiment[23]
$^2S_{1/2}$	0.0000000	0.0000000	$^2S_{1/2}$	0.0000000

The next set of tables shows multiplet energy comparisons for carbon, nitrogen, oxygen, aluminum, silicon, titanium, and chromium.

Table 2. Carbon multiplet energies (eV)

Term Symbol	OLCAO-DVME Method	DVME	Term Symbol	Experiment [24]
$^3P_{0,1,2}$	0.000000	0.000000	$^3P_0$	0.0000000
	0.000000	0.000592	$^3P_1$	0.002035413
	0.000000	0.001132	$^3P_2$	0.005382583
$^1D_2$	1.506279	1.947265	$^1D_2$	1.263728
	1.506279	1.948595		
	1.506279	1.948948		
	1.506279	1.949887		
	1.506279	1.951090		
$^1S_0$	3.765696	4.8720310	$^1S_0$	2.684014

For carbon, there are three low energy term symbols that may be obtained via transition from the $[He]2s^22p^2$ ground state: ^3P, ^1D, and ^1S. Again, the superscript defines the spin configuration for each term symbol, and the number of energy values for each term symbol letter is determined by the number of orbitals of the same angular momentum combined with the anti-symmetric requirement. For instance, ^3P (read as 'triplet P') has three J values shown due to the possible allowed combinations of electron spin and orbital angular momenta that lead to anti-symmetric wave functions. Specifically, the ^3P has two parallel (symmetric) spins for a total S equal to one. Each electron has an orbital angular momentum

of one such that the total L may take on values of 2, 1, or 0. Consequently, based only on the addition of angular momentum via LS coupling, the possible J values are 3, 2, 1, or 0. Further refining this list to produce only anti-symmetric configurations leads to $S=1$, $L=1$ so that $J=2,1,0$.

The energetic differences among the ^{3}P states that are expressed in the NIST data are the result of spin-orbit coupling while the differences in the pure DVME data are the result of integration error. For the $^1D_2$ case the energy levels should possess orbital degeneracy and so only one is listed in the NIST data. As with the ^{3}P case, the energy differences in the stand-alone DVME results are due to integration error. This may be contrasted with the hybrid OLCAO-DVME results which show perfect degeneracy for all five orbitals.

The trends for atomic C continue with the other elements. Orbital degeneracies that are not due to spin-orbit coupling are exactly represented in the OLCAO-DVME method but not the stand-alone DVME method. Orbital degeneracies in the NIST data are reflected by only one number, but spin-orbit splittings are shown. There are some further anomalies that appear for higher Z atoms which will be discussed next.

Table 3. Nitrogen multiplet energies (eV)

Term Symbol	OLCAO-DVME Method	DVME	Term Symbol	Experiment[24]
$^4S_{3/2}$	0.000000	0.000000	$^4S_{3/2}$	0.000000
$^2D_{5/2,3/2}$	2.706276	3.199266	$^2D_{5/2}$	2.383523
	2.706276	3.199597	$^2D_{3/2}$	2.384610
	2.706276	3.201109		
	2.706276	3.201610		
	2.706276	3.203819		
$^2P_{1/2,3/2}$	4.510460	5.334013	$^2P_{1/2}$	3.575570
	4.510460	5.334013	$^2P_{3/2}$	3.575618
	4.510460	5.334790		

Table 4. Oxygen multiplet energies (eV)

Term Symbol	OLCAO-DVME Method	DVME	Term Symbol	Experiment[24]
$^3P_{0,1,2}$	0.000000	0.000000	$^3P_0$	0.000000
	0.000000	0.003016	$^3P_1$	0.019622
	0.000000	0.003738	$^3P_2$	0.028142
$^1D_2$	2.109835	2.346584	$^1D_2$	1.967364
	2.109835	2.351542		
	2.109835	2.352462		
	2.109835	2.353076		
	2.109835	2.355483		
$^1S_0$	5.274588	5.876203	$^1S_0$	4.189746

Table 5. Aluminum multiplet energies (eV)

Term Symbol	OLCAO-DVME Method	DVME	Term Symbol	Experiment [25,26]
$^2P_{1/2,3/2}$	0.000000	0.000000	$^2P_{1/2}$	0.000000
	0.000000	0.001079	$^2P_{3/2}$	0.013894
	0.000000	0.002662		

Table 6. Silicon multiplet energies (eV)

Term Symbol	OLCAO-DVME Method	DVME	Term Symbol	Experiment [27]
$^3P_{0,1,2}$	0.000000	0.000000	$^3P_0$	0.000000
	0.000000	0.000540	$^3P_1$	0.009561
	0.000000	0.002883	$^3P_2$	0.027668
$^1D_2$	1.126786	1.477118	$^1D_2$	0.780958
	1.126786	1.479868		
	1.126786	1.480659		
	1.126786	1.481468		
	1.126786	1.483393		
$^1S_0$	2.816966	3.699545	$^1S_0$	1.908659

Table 7. Titanium multiplet energies (eV)

Term Symbol	OLCAO-DVME Method	DVME	Term Symbol	Experiment [28]
$^3F_{2,3,4}$	0.000000	0	$^3F_2$	0.000000
	0.000000	0.00623	$^3F_3$	0.021094
	0.000000	0.00741	$^3F_4$	0.047967
	0.000000	0.01103		
	0.000000	0.01238		
	0.000000	0.02707		
	0.000010	0.02917		
$^5F_{1,2,3,4,5}$	0.895369	0.41582	$^5F_1$	0.8129437
	0.895380	0.41729	$^5F_2$	0.8181426
	0.895380	0.43587	$^5F_3$	0.82585948
	0.895380	0.43665	$^5F_4$	0.83599519
	0.895390	0.43999	$^5F_5$	0.8484192
	0.895390	0.44031		
	0.895390	0.44827		
$^1D_2$	1.13099	1.61907	$^1D_2$	0.8995494
	1.13099	1.62392		
	1.13099	1.62488		
	1.13099	1.69335		
	1.13099	1.70036		
$^3P_{0,1,2}$	1.32576	1.70226	$^3P_0$	1.0460073
	1.32576	1.70889	$^3P_1$	1.05292613
	1.32576	1.71082	$^3P_2$	1.06655473
$^3F_{2,3,4}$	-	-	$^3F_2$	1.42975613
	-	-	$^3F_3$	1.44315261
	-	-	$^3F_4$	1.46013858
	-	-		
	-	-		
	-	-		
	-	-		
$^1G_4$	1.78897	1.79972	$^1G_4$	1.5024892
	1.78897	1.81572		
	1.78897	1.8181		
	1.78898	2.0627		
	1.78898	2.06429		
	1.78898	2.06667		
	1.78898	2.067		
	1.78898	2.0705		
	1.78898	2.07094		
$^5P_{1,2,3}$	-	-	$^5P_1$	1.7335189
	-	-	$^5P_2$	1.7393044
	-	-	$^5P_3$	1.7488757

Table 8. Chromium multiplet energies (eV)

Term Symbol	OLCAO-DVME Method	DVME	Term Symbol	Experiment [29]
$^7S_3$	0.000000	0.000000	$^7S_3$	0.000000
$^5S_2$	2.11166	2.60561	$^5S_2$	0.941430
$^5D_{0,1,2,3,4}$	-	-	$^5D_0$	0.96097008
	-	-	$^5D_1$	0.96841323
	-	-	$^5D_2$	0.98287741
	-	-	$^5D_3$	1.00367492
	-	-	$^5D_4$	1.03000806
$^5G_{2,6,3,4,5}$	3.23514	2.69414	$^5G_2$	2.543836
	3.23514	2.69571	$^5G_6$	2.544100
	3.23514	2.70899	$^5G_3$	2.544268
	3.23514	2.71366	$^5G_4$	2.544606
	3.23514	2.72786	$^5G_5$	2.544639
	3.23514	3.82348		
	3.23514	3.82364		
	3.23514	3.82457		
	3.23514	3.82532		
$^5P_{3,2,1}$	3.66658	3.82683	$^5P_3$	2.707915
	3.66658	3.82789	$^5P_2$	2.708786
	3.66658	3.82918	$^5P_1$	2.709914
$^3P_{0,1,2}$	-	-	$^3P_0$	2.87187330
	-	-	$^3P_1$	2.91511321
	-	-	$^3P_2$	2.98716592
$^7P^o_{2,3,4}$	-	-	$^7P^o_2$	2.88945204
	-	-	$^7P^o_3$	2.89953683
	-	-	$^7P^o_4$	2.91348179
$^3H_{4,5,6}$	-	-	$^3H_4$	2.96741994
	-	-	$^3H_5$	2.98256886
	-	-	$^3H_6$	3.00044213
$^5D_{0,4,1,2,3}$	3.78868	3.83034	$^5D_0$	3.00997113
	3.78868	3.83181	$^5D_4$	3.01062750
	3.78868	4.34235	$^5D_1$	3.01114739
	3.78868	4.34514	$^5D_2$	3.01279639
	3.78868	4.34819	$^5D_3$	3.01329984

In each case shown, multiplet energies from the hybrid method match experimental values more closely than do their DVME counterparts, in terms of magnitude and degeneracy. Whereas the term symbols for a carbon atom are relatively straightforward to tabulate, the production of term symbols for higher-Z atoms like titanium and chromium is extremely complicated. However, the general rules explained above can be extended to treat generation higher-Z atoms [30].

Both sets of calculations (OLCAO-DVME hybrid method and stand-alone DVME method) were non-relativistic, so spin-orbit coupling was not taken into account. This explains why the experimental multiplet energy values are resolved according to individual term symbols (with differing magnitudes), and the multiplet energy values computed via the hybrid method are the same for a given term symbol letter. The improved agreement with respect to magnitude and degeneracy is a significant step forward because it demonstrates that the basic approach is sound and that additional improvements should be possible with the inclusion of higher-order theory. However, the above results also reveal limitations in the approach that will require further investigation before they can be fully resolved.

The multiplet energies shown for titanium and chromium are a subset of the total list of values produced; the hybrid method produced 225 multiplet energy values for titanium, and 400 for chromium. The full list of multiplet energy values for titanium and chromium is contained in an external appendix that is available with this document. The multiplet energy values shown for titanium and chromium convey that the hybrid method is capable of producing some of the multiplet energies with expected degeneracies and magnitudes, compared to experimental values. However, the method is insufficient to produce all the experimentally observed excited-state multiplets. The Cr $^5D_{0,1,2,3,4}$ (quintuplet D) state is not reproduced in the correct energetic order by either the stand-alone DVME method or the hybrid OLCAO-DVME method. The energy levels *are* computed (and can be seen in the full list of energy levels in the supplementary appendix available with this document), but their energies are much higher than experiment indicates. The precise reason for this discrepancy is unknown, but because the problem manifests itself primarily with configurations that include a significant *4s* orbital component it may be surmised that the basis function for that orbital is less than ideal. Likely, it is too compact. The effect of a compact orbital is to force the 4s electronic states to be too close to other orbitals, thus raising their energy primarily through Coulombic repulsion.

4. Conclusion

The application of the DFT-CI hybrid method related in this dissertation has yielded promising results evidenced by the experimentally accurate atomic energy levels shown the preceding calculations. Although the energy levels of single atoms have been accurately computed before with tools like GRASP2K [31,32], and the computation of multiplet energy levels of multi-atom clusters has also been possible, the important contribution of the formalism exhibited here is that it is extendable to treat multi-atom solids. Therefore, a major advance from this work is that a door is now opened to the computation of multiplet energy levels of wave functions that are expressed in terms of Bloch waves instead of just atomic orbitals or molecular orbitals as found in most other methods. Along the way, re-derivation of the existing interaction integrals in the OLCAO package has led to increased accuracy. For example, re-deriving the momentum matrix integrals rectified a long-standing problem that hampered the computation of the dielectric function and energy-loss function of high-Z atom containing materials.

Acknowledgements

I wish to express gratitude to my advisor, Dr. Paul Rulis. His patience, support, and encouragement have been an essential part of my work. A very special thanks to Dr. Kazuyoshi Ogaswara of Kwansei Gakuin University; his research experience and zeal have inspired me.

References

[1] Zunger, A., Wagner, S. & Petroff, P. M. New Materials and Structures for Photovoltaics. J. Electron. Mater. 22, 3–16 (1993).
[2] Atherton, L. J., Payne, S. A. & Brandle, C. D. Oxide and Fluoride Laser Crystals. Annu. Rev. Mater. Sci. 23, 453–502 (1993).
[3] Antoni, R. Heterostructure Infrared Photovoltaic Detectors. Infrared Phys. Technol. 41, 213–238 (2000).
[4] Lin, C. C. & Liu, R.-S. Advances in Phosphors for Light-emitting Diodes. J. Phys. Chem. Lett. 2, 1268–1277 (2011).
[5] Ramsay, A. J. A Review of the Coherent Optical Control of the Exciton and Spin States of Semiconductor Quantum Dots. Semicond. Sci. Technol. 25, 103001 (2010).
[6] Cocoletzi, G. H. & Mochán, W. L. Excitons: From Excitations at Surfaces to Confinement in Nanostructures. Surf. Sci. Rep. 57, 1–58 (2005).
[7] Buse. Light-Induced Charge Transport Processes in Photorefractive Crystals I: Models and Experimental Methods. Appl. Phys. B Lasers Opt. 64, 273–291 (1997).
[8] Shen, Z.-X. & Dessau, D. S. Electronic Structure and Photoemission Studies of Late Transition-

Metal Oxides — Mott Insulators and High-Temperature Superconductors. Phys. Rep. 253, 1–162 (1995).
[9] Huang, P. & Carter, E. A. Advances in Correlated Electronic Structure Methods for Solids, Surfaces, and Nanostructures. Annu. Rev. Phys. Chem. 59, 261–290 (2008).
[10] Klepeis, J. E. Introduction to First-Principles Electronic Structure Methods: Application to Actinide Materials. J. Mater. Res. 21, 2979–2985 (2006).
[11] Ohnishi, S. & Sugano, S. Theoretical Studies of High-Pressure Effects on Optical Properties of Ruby. Jpn. J. Appl. Phys. 21, L309–L311 (1982).
[12] Ogasawara, K. et al. Analysis of Covalent Effects on the Multiplet Structure of Ruby Based on First-Principles Cluster Calculations. Jpn. J. Appl. Phys. 37, 4590–4594 (1998).
[13] Tomohiko Ishii, Hisanobu Wakita, Kazuyoshi Ogasawara, & Yang-Soo Kim. The DV-Xα Molecular-Orbital Calculation Method. (Springer International Publishing, 2015).
[14] Fairbank, W. M., Klauminzer, G. K. & Schawlow, A. L. Excited-State Absorption in Ruby, Emerald, and MgO:Cr3+. Phys. Rev. B 11, 60–76 (1975).
[15] Tanabe, Y. & Sugano, S. On the Absorption Spectra of Complex Ions. I. J. Phys. Soc. Jpn. 9, 753–766 (1954).
[16] Tanabe, Y. & Sugano, S. On the Absorption Spectra of Complex Ions II. J. Phys. Soc. Jpn. 9, 766–779 (1954).
[17] Multiplets of Transition-Metal Ions in Crystals - 1st Edition. Available at: https://www.elsevier.com/books/multiplets-of-transition-metal-ions-in-crystals/sugano/978-0-12-676050-7. (Accessed: 14th December 2017)
[18] Ogasawara, K., Ishii, T., Tanaka, I. & Adachi, H. Calculation of Multiplet Structures of Cr^{3+} and V^{3+} in α-Al_2O_3 Based on a Hybrid Method of Density-Functional Theory and the Configuration Interaction. *Phys. Rev. B* **61,** 143 (2000).
[19] Ching, W. Y. Theoretical Studies of the Electronic Properties of Ceramic Materials. *J. Am. Ceram. Soc.* **73,** 3135–3160 (1990).
[20] Ogasawara, K. & Watanabe, S. Chapter 22 Current Situation and Future Development of Discrete Variational Multielectron Method. in *Advances in Quantum Chemistry* **Volume 54,** 297–314 (Academic Press, 2008).
[21] Ching, W.-Y. & Rulis, P. *Electronic Structure Methods for Complex Materials: The Orthogonalized Linear Combination of Atomic Orbitals*. (Oxford University Press, USA, 2012).
[22] Griffiths, D. J. *Introduction to Quantum Mechanics*. (Pearson Prentice Hall, 2004).
[23] Sansonetti, J. E. Wavelengths, Transition Probabilities, and Energy Levels for the Spectra of Sodium (NaI–NaXI). *J. Phys. Chem. Ref. Data* **37,** 1659–1763 (2008).
[24] Tables of Spectra of Hydrogen, Carbon, Nitrogen, and Oxygen Atoms and Ions. *CRC Press* (1993). Available at: https://www.crcpress.com/Tables-of-Spectra-of-Hydrogen-Carbon-Nitrogen-and-Oxygen-Atoms-and-Ions/Gallagher-Moore/p/book/9780849374203. (Accessed: 9th August 2017)
[25] Martin, W. C. & Zalubas, R. Energy levels of aluminum, Al I through Al XIII. *J. Phys. Chem. Ref. Data* **8,** 817–864 (1979).
[26] Kaufman, V. & Martin, W. C. Wavelengths and Energy Level Classifications for the Spectra of Aluminum (Al I through Al XIII). *J. Phys. Chem. Ref. Data* **20,** 775–858 (1991).
[27] Martin, W. C. & Zalubas, R. Energy Levels of Silicon, Si I through Si XIV. *J. Phys. Chem. Ref. Data* **12,** 323–380 (1983).
[28] Saloman, E. B. Energy Levels and Observed Spectral Lines of Neutral and Singly Ionized Titanium, Ti I and Ti II. *J. Phys. Chem. Ref. Data* **41,** 013101-013101-116 (2012).
[29] Saloman, E. B. Energy Levels and Observed Spectral Lines of Neutral and Singly Ionized Chromium, Cr I and Cr II. *J. Phys. Chem. Ref. Data* **41,** 043103 (2012).
[30] Hyde, K. E. Methods for Obtaining Russell-Saunders Term Symbols from Electronic Configurations. *J. Chem. Educ.* **52,** 87 (1975).
[31] Jönsson, P., He, X., Froese Fischer, C. & Grant, I. P. The grasp2K Relativistic Atomic Structure Package. *Comput. Phys. Commun.* **177,** 597–622 (2007).

[32] Jönsson, P., Li, J., Gaigalas, G. & Dong, C. Hyperfine Structures, Isotope Shifts, and Transition Rates of C II, N III, and O IV from Relativistic Configuration Interaction Calculations. *At. Data Nucl. Data Tables* **96,** 271–298 (2010).